

## Sequence of dielectric anomalies and high-temperature relaxation behavior in $\text{Na}_{1/2}\text{Bi}_{1/2}\text{TiO}_3$

C.-S. Tu, I. G. Siny,\* and V. H. Schmidt

*Department of Physics, Montana State University, Bozeman, Montana 59717*

(Received 7 September 1993; revised manuscript received 21 December 1993)

Measurements of relative permittivity ( $\epsilon = \epsilon' - i\epsilon''$ ) in the complex perovskite crystal  $\text{Na}_{1/2}\text{Bi}_{1/2}\text{TiO}_3$  were carried out as functions of frequency (0.02–300 kHz) and temperature (300–900 K) in both heating and cooling processes. We have found three anomalies separating four different temperature regions. In order of decreasing temperature, the first anomaly centered near 800 K is a smooth but rapid increase in low-frequency (< 50 kHz) permittivity to very high values of order  $1 \times 10^5$ , associated with the cubic to tetragonal transition. This high permittivity shows considerable dispersion and decreases quite rapidly as temperature drops from 860 to 640 K. We attribute this large permittivity to superparaelectric clusters, and their slow relaxation to random electric fields from randomly placed  $\text{Na}^+$  and  $\text{Bi}^{3+}$  ions which redistribute and allow cluster reversal with the  $\rho\epsilon_0\epsilon'_{dc}$  time constant determined by the conductivity and permittivity. The other anomalies, seen previously by others, are a high-frequency permittivity (50 to 300 kHz) which shows no dispersion and increases slowly down to a peak of  $3 \times 10^3$  near 640 K, where a trigonal phase exhibiting antiferroelectric and/or incommensurate characteristics is reported to set in. It then drops and develops weak low-frequency dispersion below 550 K which is the upper limit reported for spontaneous polarization decay.

### I. INTRODUCTION

Sodium bismuth titanate  $\text{Na}_{1/2}\text{Bi}_{1/2}\text{TiO}_3$  (NBT) was discovered to be a ferroelectric at room temperature with a dielectric peak attributed at that time to a Curie temperature near 593 K.<sup>1</sup> One more phase transition at a lower temperature was also assumed because of some additional anomalies in both the dielectric constant and linear thermal expansion coefficient.<sup>2,3</sup> Since then NBT has attracted considerable attention, different dielectric anomaly studies have been published in a number of papers,<sup>2–12</sup> but its behavior is still far from clear. Most of the contradictions concern the number and location of different phases as well as the electrical state in each phase. According to x-ray and neutron measurements<sup>6,9,13</sup> there are two structural phase transitions in NBT from the high-temperature cubic phase to a tetragonal and then a trigonal phase. The sequence of electric order transformations from a cubic paraelectric state to a ferroelectric state at room temperature passes through some phases whose nature and properties are not well understood. The tetragonal phase seems to be ferroelastic (as was shown by domain pattern visualization) (Ref. 7) without any dielectric anomaly at the transition from a cubic phase. However, the question of whether this phase is polar is still open. Our dielectric results support the idea that this phase is superparaelectric rather than truly polar. Much of the unexplained behavior has been found in the range between the ferroelastic and ferroelectric phases.<sup>9</sup> Some dielectric measurements indicate that an antiferroelectric phase exists between the tetragonal ferroelastic and trigonal ferroelectric phases.<sup>2,5</sup> However, x-ray<sup>6</sup> and neutron-scattering studies<sup>13</sup> have not provided any evidence in support of this view. Neutron scattering indicates that the transition between tetragonal and trigonal phases is characterized by a region of phase

coexistence. A new designation LTNP (low-temperature nonpolar) was proposed for this phase.<sup>9</sup> However, this new label reveals neither the structure nor the role of this phase in the evolution of electrical properties. Thus, the nature of the high-frequency dielectric maximum near 640 K is still an open question.

Most dielectric measurements in NBT have been carried out at relatively high frequencies. Because NBT is considered to be a relaxor ferroelectric, measurements at low and ultralow frequencies are absolutely essential. For example, the existence of slow processes in NBT was indicated by the time dependence of the dielectric constant just in the mysterious region discussed above.<sup>10,11</sup> We report here our measurements of  $\epsilon(f, T)$  at audio frequencies as a first step in studying such slow processes.

We also examined old and recent results showing the existence of an antiferroelectric-ferroelectric pair of transitions in other perovskite-type complex materials.<sup>14–16</sup> This coupled pair of transitions appears to play a special role in relaxor ferroelectric dynamics. Even  $\text{PbSc}_{1/2}\text{Ta}_{1/2}\text{O}_3$  which has an ordinary diffuse ferroelectric phase transition revealed a modulated antiferroelectric state at higher temperature in transmission electron microscopy.<sup>17</sup> This provided another motivation for our reexamination of the phase-transition sequence in NBT by dielectric measurements.

### II. EXPERIMENTAL PROCEDURE

In our experiments a single NBT crystal grown by the Czochralski method, with dimensions  $5.57 \times 6.03 \times 5.74$  (mm)<sup>3</sup>, was electroded with silver paste (Ted Pella #16032). The capacitance and conductance were measured with a field near 0.8 V/cm using a Wayne-Kerr Model 6425 Precision Component Analyzer with four-lead connections. The measuring accuracy is about

$\pm 0.05\%$ . A LakeShore PT-103 platinum resistance thermometer calibrated for high temperature was put just above the sample in the oven. The temperature accuracy is about  $\pm 0.1$  K. All data were collected automatically with frequency swept in steps from 0.02 to 300 kHz. The sample was heated first from room temperature to 900 K at a rate of  $1.7 \pm 0.2$  K/min, and then cooled at the same rate. The crystal was kept at 900 K about 10 min before cooling began. Results from several heating-cooling cycles were found to be reproducible.

### III. EXPERIMENTAL RESULTS

Figure 1 reveals a new large anomaly at higher temperature. In comparison with this anomaly, the "old" and well-known anomalies in the temperature regions indicated by arrows *A* and *B* in Fig. 1 are very small. However, our data agree with most published results in the *A* and *B* regions. The new anomaly in the *C* region was not seen previously because neither low frequencies nor high temperatures were used in the former measurements. We will consider separately each of these three regions.

#### A. Anomaly at the Curie temperature (region *A*)

This anomaly was found by Smolensky *et al.*<sup>1</sup> and later by others,<sup>2-4,8,10-12</sup> sometimes with substantial modifications.<sup>6,7,9</sup> At frequencies below 200 Hz we could hardly see this anomaly against the large background of dielectric permittivity. It appears as a pronounced shoulder in the region  $0.2 < f < 1$  kHz (Fig. 2 inset). In Fig. 2, we compare our measurements at 100 kHz (two curves labeled 1) with published data. The two curves labeled 2 at 500 kHz were also measured on a NBT single crystal and appeared in several papers by Pronin *et al.*<sup>3,4,8</sup>

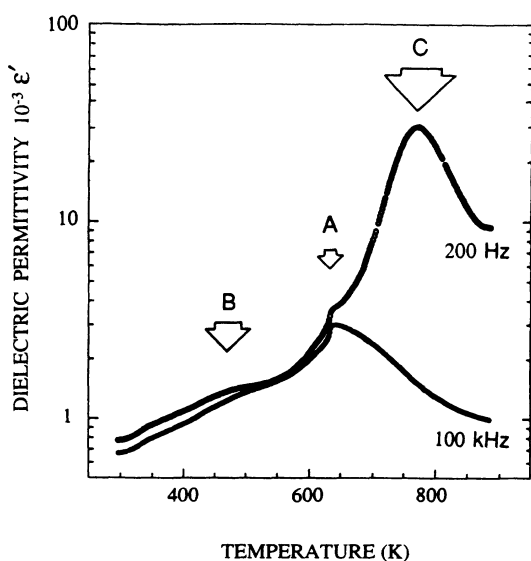


FIG. 1. The temperature dependence of the real part of the dielectric relative permittivity in NBT at two frequencies upon heating. The *A*, *B*, and *C* arrows indicate three anomalous regions.

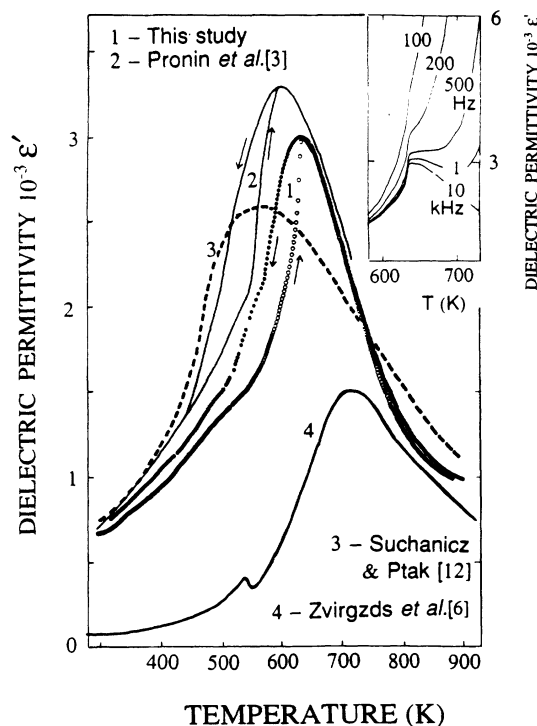


FIG. 2. Comparison of the dielectric anomaly in region *A*. Curves 3 and 4 show only heating and cooling runs, respectively. The inset shows that this anomaly is hidden by an increasing background at lower frequencies.

These two sets of data agree well in the peak value and in the specific difference in behavior on the left side of the  $\epsilon'$  peak in heating and cooling runs. Curve 3 (at 160 kHz) reproduces a recent result for a NBT single crystal by Suchanicz *et al.*<sup>10-12</sup> which is quite different from our data. Curve 4 in Fig. 2 represents very different behavior of NBT ( $f = 200$  kHz) taken from Ref. 6. The difference for lower frequencies is even more unusual.<sup>6</sup> We attribute these differences to sample quality, and consider our NBT sample to be of good quality. A significant change in both the size and shape of this anomaly after annealing confirms the sensitivity of this anomaly to the variation of local structure.<sup>7</sup>

Our measurements in the frequency range 0.1–100 kHz show no evident dispersion for the peak position (Fig. 1 and Fig. 2 inset) and are in agreement with most other results.<sup>2,3,7</sup> Except for the unusual data<sup>6</sup> shown in curve 4 of Fig. 2, only one paper<sup>12</sup> shows some dispersion for the  $\epsilon'(f, T)$  peak position in the high-frequency region ( $f \geq 160$  kHz). Thus, there is little evidence that the dielectric anomaly at the Curie temperature in NBT corresponds to the typical dielectric anomaly in relaxor ferroelectrics which has dispersion as a main characteristic feature.<sup>18</sup>

#### B. A small anomaly at lower temperatures (region *B*)

Smolensky *et al.*<sup>1</sup> also noted an additional phase transformation in NBT below the Curie temperature by analyzing anomalies in the linear thermal expansion coefficient. Later, a dielectric permittivity anomaly was

found at nearly the same temperature, where the permittivity develops dispersion and begins to decrease more slowly with decreasing temperature.<sup>2,3</sup> Remanent polarization disappears above 550 K,<sup>2,12</sup> as shown in Fig. 3, so this dispersion can be attributed to domain wall displacement. Our measurements agree perfectly with those previous measurements<sup>2,3,12</sup> and indirectly confirm the onset of ferroelectric behavior below 550 K.

The above two anomalies (*A* and *B*) in the  $\epsilon'$  behavior demarcate an enigmatic phase in NBT. Evidence for antiferroelectric behavior of this phase includes typical double hysteresis loops at temperatures between the *B* and *A* dielectric anomalies and characteristic changes in  $\epsilon'$  due to dc biasing fields and in initially polarized samples.<sup>2-5</sup> However, a recent paper<sup>12</sup> suggests that no antiferroelectric phase occurs in NBT. We believe we have succeeded in explaining this contradiction, taking into account that this tandem of dielectric anomalies in NBT shows similarity to those in other complex perovskites like  $\text{PbCo}_{12}\text{W}_{1/2}\text{O}_3$  and  $\text{PbYb}_{1/2}\text{Ta}_{1/2}\text{O}_3$ . These arguments will be considered in Sec. IV.

### C. A new anomaly at higher temperatures (region C)

A huge frequency-dependent peak for the real part  $\epsilon'$  of the dielectric permittivity was found in the higher-temperature region [Figs. 1, 4, and 5(a)]. A corresponding  $\epsilon''$  contribution appears as a shoulder added to the conductivity contribution to the imaginary part of the permittivity [Fig. 5(b)]. The growth in  $\epsilon''$  was drastic enough to arouse suspicion about the correctness of the  $\epsilon'$  measurements. To check their correctness, we compared the dielectric measurements in NBT and in a sample of the well-known relaxor ferroelectric  $\text{PbMg}_{1/3}\text{Nb}_{2/3}\text{O}_3$  (PMN) under similar conditions. As shown in Fig. 5, at high temperatures above  $\sim 800$  K at nearly the same level of  $\epsilon''$  we did not find a pronounced peak in  $\epsilon'$  for PMN [Fig. 5(a)]. We conclude that the huge peak of  $\epsilon'$  in NBT is not an artifact. The hump in the imaginary part of the permittivity for NBT in Fig. 5(b) is only seen clearly at

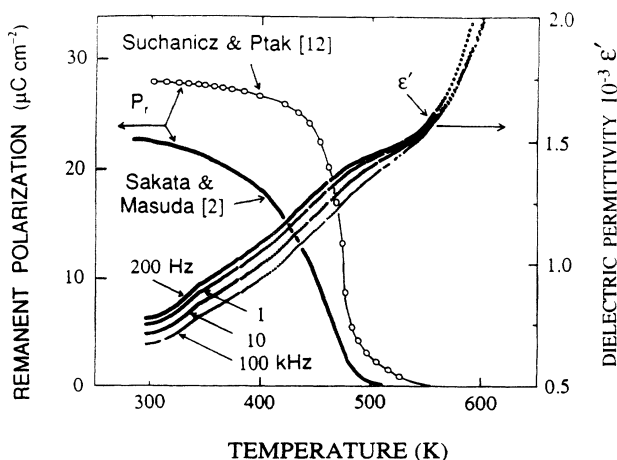


FIG. 3. The temperature dependences of remanent polarization,  $P_r$ , and dielectric permittivity ( $\epsilon'$ ) upon heating in region *B* where a ferroelectric state exists.

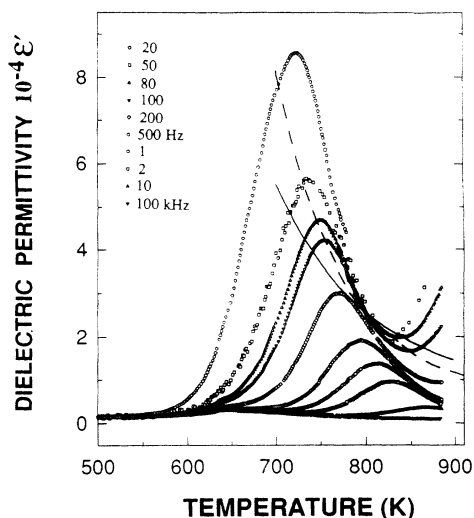


FIG. 4. The real part of dielectric permittivity vs temperature in region *C* at various frequencies upon heating. The solid line is the calculation of Eq. (5) with  $N = 54$  and dashed line is the calculation of Eq. (5) with  $N = 125$ .

frequencies below 1 kHz. By comparing Figs. 5(a) and 5(b), it is clear that this hump in  $\epsilon''$  is due to a relaxation-type mechanism. The humps for various frequencies are separated from the conductivity contribution in Fig. 6(b).

The large  $\epsilon''$  at high temperature due to the conductivity does seem to cause an artifact in Figs. 4 and 5(a), namely, the turning upward of the  $\epsilon'$  curves at the

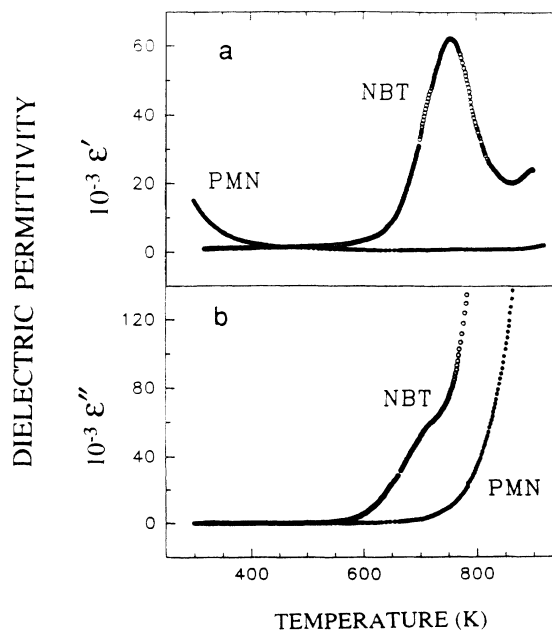


FIG. 5. (a) The temperature dependence of the real part ( $\epsilon'$ ) of the dielectric permittivity in NBT and PMN at 100 Hz upon cooling. (b) The temperature dependence of the imaginary part ( $\epsilon''$ ) of the dielectric permittivity in NBT and PMN at 100 Hz upon cooling.

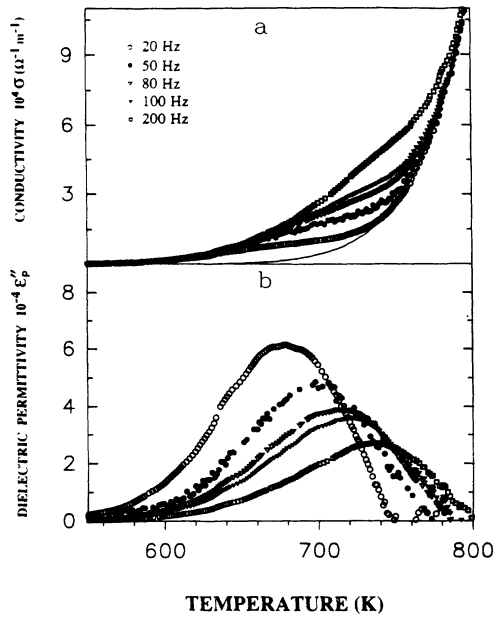


FIG. 6. (a)  $\sigma (=2\pi f\epsilon_0\epsilon'')$  vs temperature at five different frequencies. The solid line is the fit of Eq. (2) for  $\sigma_c$  with parameters  $\sigma_0=2.12\times 10^7$  ( $\Omega\text{m}$ ) $^{-1}$  and  $W=18\,860$  K. (b) The imaginary part of dielectric permittivity,  $\epsilon_p''=\Delta\sigma/(2\pi f\epsilon_0)$  vs temperature at five different frequencies. Here  $\Delta\sigma=\sigma-\sigma_c$ .

highest temperatures. One sees in Fig. 4 that this turning upward occurs to the right of the envelope of the  $\epsilon'$  curves for various frequencies. We believe that all these curves, when they come in from the left and meet this envelope, should follow the envelope down and to the right. This envelope represents the dc permittivity. We attribute the origin of the upward-curving lines to the right of the envelope to a slight experimental error in phase angle of the permittivity  $\epsilon'-i\epsilon''$ . If  $\epsilon''$  is ten times as large as  $\epsilon'$ , then a 0.01 rad (0.6°) error in the direction of  $\epsilon$  in the complex plane will cause a 10% error in the  $\epsilon'$  value. The beginning of the observed upturn away from the dc  $\epsilon'$  envelope actually occurs near  $\epsilon''=10\epsilon'$  for all frequencies exhibiting this upturn. We did not erase these upturns from these figures because we want to emphasize the importance of watching out for artifacts of this type.

The next step in the data presentation assumes that the electrical response has two parts: (1) the frequency-independent (probably ionic) conductivity response of free charges, and (2) the frequency-dependent polarization response of bound charges.

The free carrier response can have frequency dependence, but over our frequency range a frequency-independent response appears consistent with the experimental results.

Based on these assumptions, the permittivity is

$$\epsilon=\epsilon'-i\epsilon''=\epsilon'_p-i(\epsilon''_p+\epsilon''_c), \quad \epsilon''_c=\frac{\sigma_c}{2\pi f\epsilon_0}, \quad (1)$$

$$\sigma_c=\sigma_0e^{-W/T}. \quad (2)$$

Here the  $p$  and  $c$  subscripts refer to polarization and

conductivity contributions,  $\epsilon_0$  is the MKS (meter-kg-sec) system permittivity constant,  $f$  is the measurement frequency, and we assume a thermally activated conductivity. We obtained  $\sigma_0=2.12\times 10^7$  S/m and  $W=18\,860$  K by fitting the portion of the lowest-frequency (20 Hz) data in Fig. 6(a) which coincides with higher-frequency data and thus represents the frequency-independent contribution from the conductivity.

The raw  $\sigma (=2\pi f\epsilon_0\epsilon'')$  data and the above fit to the conductivity (which corresponds to  $\sigma_c$  on the graph) appear in Fig. 6(a). The remainder  $\epsilon_p''$  curves for various frequencies left after subtracting the conductivity contribution appear in Fig. 6(b).

This analysis allows us to identify Figs. 4 and 6(b) as the respective real and imaginary parts of the polarization contribution to the permittivity. Cole-Cole plots based on these data appear in Fig. 7 for temperatures of 600, 650, 700, and 750 K. All these plots have the typical semicircular shape, with the circle center somewhat below the real axis. Extrapolation of these circular arcs clockwise to the real axis provides estimated dc permittivity at 650 and 700 K, at which temperatures the polarization could not develop the full dc response at the lowest frequency of 20 Hz. Extrapolation at 620, 630, and 640 K (data not shown) indicates that dc permittivity drops as temperature decreases below 640 K, but the limited arc length for these data limit the accuracy of these extrapolations.

Figure 8 compares permittivity peak location and magnitude for heating and cooling runs. The  $\epsilon'$  peaks occur at the same temperature upon heating and cooling at 100 Hz and 10 kHz. For 1 kHz the heating run peak is at 813 K while the cooling run peak is at 800 K. We attribute this difference to a slight thermal hysteresis in the cubic-tetragonal ferroelastic phase transition found<sup>13</sup> at 820 K, although no hysteresis was reported for that transition in their neutron-diffraction study.

This transition is also the probable reason for the drop in the 800–830 K range of the difference  $[\Delta J/(J_h+J_c)]$ ,  $\Delta J=J_c-J_h$  in peak  $\epsilon'$  magnitudes upon heating ( $J_h$ ) and cooling ( $J_c$ ) shown for several frequencies in the upper right inset of Fig. 8. We speculate that upon cool-

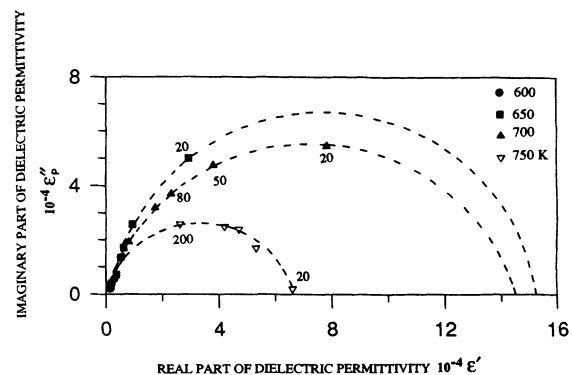


FIG. 7. Complex representation of the NBT dielectric permittivity at four different temperatures. The numbers on the points indicate the frequencies in Hz. The dashed lines are regression lines.

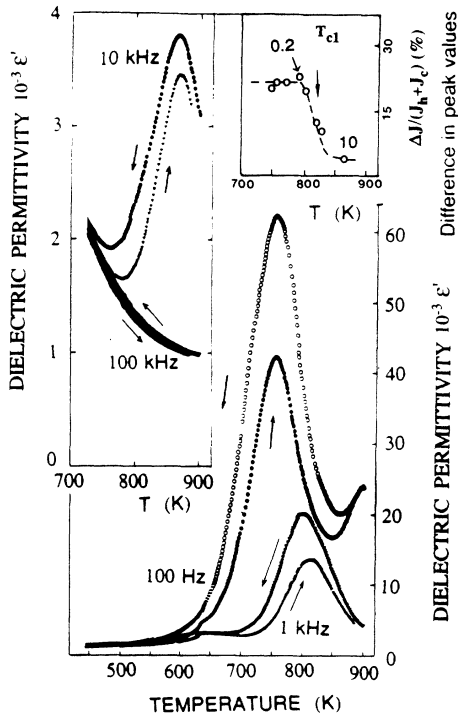


FIG. 8. The strong thermal hysteresis behavior in region C at four different frequencies (10 and 100 kHz in the left inset). Right inset: the difference of heating and cooling peak values shows a drop in the region of the ferroelastic phase transition at  $T_{c1} \sim 820$  K. The numbers on the points indicate the frequencies in kHz. The dashed line is a regression line.

ing from the cubic phase, the ferroelastic domains which form in the tetragonal phase are larger, while upon heating from the trigonal phase they are smaller and have a greater tendency to limit the size of the superparaelectric clusters discussed in the following section. This size limitation would cause the observed weaker permittivity response upon heating.

#### IV. ANALYSIS AND DISCUSSION

The dielectric behavior must be considered in conjunction with the NBT crystal structure, particularly as there appears to be a first-order ferroelastic cubic to tetragonal transition at  $T_{c1} = 820$  K, as seen by Vakhrushev *et al.*<sup>13</sup> from neutron-diffraction measurements. The order parameter (proportional to the square root of the tetragonal  $M$ -superlattice reflection intensity) is nonzero above  $T_{c1}$ , abruptly more than doubles at  $T_{c1}$ , and gradually doubles again as temperature drops to 640 K. Below this temperature they observed rapid drop of the  $M$  reflection and rapid rise of the  $R$  (trigonal) superlattice reflection, both accompanied by about 50-K thermal hysteresis and by coexistence of the  $M$  and  $R$  reflections.

The overall dielectric response can be divided into three parts: (1) a strong lower-frequency superparaelectric response in the tetragonal phase and in the tetragonal-cubic transition region whose dynamic behavior is controlled by ionic diffusion related to the conductivity mechanism; (2) a much weaker but still

strong higher-frequency response related to the transition from tetragonal to trigonal cell shape; and (3) a ferroelectric transition in which the cell shape remains trigonal.

We consider first the superparaelectric response in the dc limit. We assume that the unit dipoles are divided into superparaelectric clusters such as those suggested by Cross<sup>19</sup> because of random placement of  $\text{Na}^+$  and  $\text{Bi}^{+3}$  cations with corresponding electric fields and elastic distortions which inhibit ferroelectric ordering of the crystal as a whole.

The behavior of the large dielectric peak at high temperature can be explained by assuming that these data lie in the crossover region from independent dipole moments to superparaelectric moments of  $N$  dipoles. In the limit  $N \rightarrow \infty$  we would have a ferroelectric phase transition. When  $N$  remains finite, as assumed here, there is a crossover region where the permittivity increases rapidly with decreasing temperature but remains finite. The permittivity  $\epsilon'$  should obey the Curie law  $\epsilon' = 1 + p^2 / (\epsilon_0 V k T)$  for independent dipoles at (unattainably) high temperature. Henceforth, we omit the 1 which is negligible for our measurements. Here  $p$  is the dipole moment of a unit cell,  $V$  is the cell volume,  $\epsilon_0$  is the MKS constant,  $k$  is Boltzmann's constant, and  $T$  is absolute temperature. At low temperature, the dc  $\epsilon'$  should obey the  $N$ -dipole-cluster Curie law  $\epsilon' = N p^2 / (\epsilon_0 V k T)$ , but the cluster reversal time for our system is too long to allow observation of the Curie-law behavior.

We attribute the rapid rise of the dc  $\epsilon'$  (the envelope of the high- $T$  sides of the  $\epsilon'$  peaks) in Fig. 4 to the crossover from the one-dipole to  $N$ -dipole Curie law. We will show that a very simple model reproduces the general shape of this envelope. The higher-temperature part of the crossover region, which we barely reached in our measurements, should obey a Curie-Weiss law  $\epsilon' = C / (T - T_0)$ . Most of our observed  $\epsilon'$  envelope lies near  $T_0$  where this  $\epsilon'$  vs  $T$  envelope becomes nearly a straight line.

The Hamiltonian for one  $N$ -dipole cluster in an electric field  $E$  is

$$H = - \sum_{i=1}^N \left[ p E S_i + J S_i \sum_{j>i} S_j \right], \quad (3)$$

where  $J$  represents a positive (ferroelectric) interaction which for mathematical and computational simplicity is assumed to exist among all dipoles in the  $N$ -dipole cluster. The mean aligned dipole excess and dc dielectric permittivity are given exactly by

$$\langle n_+ - n_- \rangle \equiv \langle 2s \rangle = \frac{\sum_{n_+=0}^N \{N/n_+\} (pE/kT) (2s)^2 e^{(4s^2 - N)J/2kT}}{\sum_{n_+=0}^N \{N/n_+\} e^{(4s^2 - N)J/2kT}}, \quad (4)$$

$$\epsilon'(f=0, T) = 1 + \frac{p \langle 2s \rangle}{N \epsilon_0 E V}, \quad (5)$$

where  $\{N/n_+\}$  represents the binomial coefficients and

$p\langle 2s \rangle / NV$  is the cluster polarization.

If  $(T - T_0)/T_0 \gg 2/N$ , where  $T_0 \equiv NJ/k$ , we can approximate the sum by an integral with limits extending to infinity, and replace the binomial coefficients by a Gaussian:

$$\langle 2s \rangle \approx \frac{(4pE/kT) \int_0^\infty s^2 e^{(2J/kT - 2/N)s^2} ds}{\int_0^\infty e^{(2J/kT - 2/N)s^2} ds}. \quad (6)$$

At higher temperature for which Eq. (6) is valid we obtain the Curie-Weiss law

$$\epsilon' \approx \frac{p^2}{\epsilon_0 V k (T - T_0)} \quad (T_0 \equiv NJ/k). \quad (7)$$

We define a dimensionless logarithmic derivative or "steepness parameter"  $S$

$$S \equiv \frac{T(d\epsilon'/dT)}{\epsilon'} = \frac{d(\ln\epsilon')}{d(\ln T)}, \quad (8)$$

which is  $-1$  in the Curie-law regions at very low and very high temperature and which should have greatest magnitude near  $T_0$ . For the Curie-Weiss law of Eq. (7) we obtain

$$S(T) = \frac{-T}{T - T_0}. \quad (9)$$

Figure 4 shows the fits for  $N = 54$  and  $125$ , with dipole moment  $p$  adjusted so that at  $800$  K these curves cross the "dc"  $\epsilon'$  curve (the curve along which low-frequency  $\epsilon'$  curves coincide). The fit is better for  $N = 125$ , but a larger  $N$  would fit still better. However, it is necessary to consider also the structural temperature dependence and its effect on the superparaelectric clusters, as will now be explained. To understand better where our data fit on the overall superparaelectric model permittivity curve, the logarithmic plot of permittivity against temperature in Fig. 9 is helpful.

The calculated superparaelectric response for  $N = 125$  dipoles in a cluster appears in Fig. 9. The  $-1$  slope regions at high temperature corresponding to independent dipoles and at low temperature corresponding to superparaelectric clusters are clearly evident. Our data, superimposed on this curve in the inset, appear only in the crossover region. The central portion of our data rises more steeply than the calculated curve but fits reasonably well, whereas there are large deviations of our data at the two ends. We now discuss how all these deviations are related to the structure, in particular to the tetragonal order parameter measured by Vakhrushev *et al.*<sup>13</sup> obtained from the neutron  $M$ -reflection intensity.

To model the effects of the transitions from cubic-to-tetragonal and tetragonal-to-trigonal phases, we assume that the number of clusters varies as the tetragonal order parameter. The tetragonal order parameter is assumed proportional to the square root of  $M$ -reflection intensity.<sup>13</sup> Multiplying the superparaelectric model permittivity of Eq. (5) by this temperature-dependent order parameter yields the calculated dc permittivity shown in the inset of Fig. 9.

Quite good agreement is seen in the inset of Fig. 9 be-

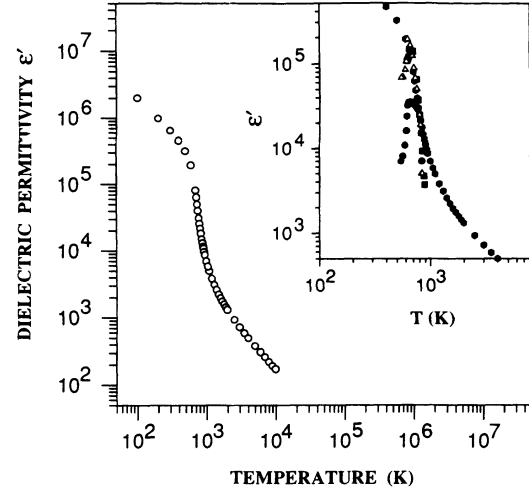


FIG. 9. The temperature behavior of dc permittivity,  $\epsilon'$ , calculated from Eq. (4) with  $N = 125$ . Inset: solid hexagons are from Eq. (4) with  $N = 125$ , squares are the "measured" dc permittivity, solid circles are proportional to the tetragonal order parameter from neutron scattering (Ref. 13), and triangles are the calculated dc permittivity as defined by the dc permittivity from Eq. (4) multiplied by the tetragonal order parameter. All curves are adjusted to cross at  $800$  K.

tween the calculated and "measured" dc permittivity. "Measured" is put in quotes because below  $750$  K the dc permittivity is found by a three-step process: First the conductivity contribution is subtracted from  $\epsilon''$  to find the polarization contribution  $\epsilon_p''$ , then Cole-Cole plots of  $\epsilon_p''$  vs  $\epsilon'$  are made, and finally the circular arcs of these plots are extrapolated clockwise until they cross the  $\epsilon'$  axis at the assumed value of dc  $\epsilon'$ . Confidence in this process is enhanced by the good fit of the data to circular arcs. Near  $600$  K the arcs become too short for accurate extrapolation. From  $750$  to  $885$  K the "measured" dc permittivity is taken as the "envelope" line in Fig. 4 along which low-frequency  $\epsilon'$  curves coincide.

It is surprising that there is no sharp increase in dc permittivity at the first-order cubic-to-tetragonal transition observed in the neutron experiment.<sup>13</sup> Neutron<sup>13</sup> and Raman<sup>20</sup> scattering exhibited a large fluctuation contribution in the cubic paraphase, and perhaps these fluctuation regions consist of incipient superparaelectric clusters which contribute strongly to the permittivity already in the cubic phase.

The parameters predicted by the superparaelectric model can be compared with those for  $\text{BaTiO}_3$  family crystals to see if they are reasonable. Fitting the model with  $N = 125$  to the dielectric data at  $800$  K we have, from the  $T$  vs  $\epsilon'$  data (Fig. 4),  $\epsilon' = 2.55 \times 10^4$ , which corresponds to a dipole moment  $p$  of  $1.12 \times 10^{-28}$  (C m) per  $0.4 \times 0.4 \times 0.4$  (nm)<sup>3</sup> unit cell, giving a Curie-Weiss constant of  $C = 1.6 \times 10^6$  K. The closest comparison can be made with  $\text{PbTiO}_3$ , which like  $\text{BaTiO}_3$  has a ferroelectric transition from a cubic to a tetragonal phase. For  $\text{BaTiO}_3$  this transition is only at  $393$  K, whereas in  $\text{PbTiO}_3$  it is at  $763$  K which is much nearer the  $820$ -K value reported by Vakhrushev *et al.* for NBT.<sup>13</sup>  $\text{PbTiO}_3$

has  $P_s = 0.75$  (C m<sup>-2</sup>) giving  $p = 4.47 \times 10^{-29}$  (C m) and has  $C = 4.1 \times 10^5$  K.<sup>18</sup> These values of  $p$  and  $C$  are about three times lower than for the above fit of the data to the superparaelectric model with  $N = 125$ . Taking another approach, we can fit the superparaelectric model with the  $p$  value from PbTiO<sub>3</sub> to the dc  $\epsilon'$  value of  $1.56 \times 10^5$  at 640 K, obtained by extrapolating the Cole-Cole curve. At this temperature the permittivity is not increasing so fast with decreasing temperature, so it is reasonable to assume that the permittivity is close to obeying the low-temperature form, i.e.,  $\epsilon' = Np^2 / (\epsilon_0 V k T)$ . We then get  $N = 391 = (7.31)^3$  which correspond to a 2.92-nm cube for a superparaelectric cluster, whereas  $N = 125 = 5^3$  correspond to a 2.00-nm cube. We conclude that we can obtain a fairly good fit with reasonable parameters if the superparaelectric moment correlation length is 2–3 nm.

The dynamic behavior of the large low-frequency peak is most strikingly illustrated by Fig. 10. Here we plot two experimental parameters against inverse temperature. One is  $\tau_{pk}$ , the inverse of the measurement angular frequency for which the  $dc\epsilon'$  peak occurs at the given temperature. These peaks are quite sharp, so this  $\tau_{pk}$  is a good approximation to the dielectric relaxation time. The other parameter plotted is the "RC" relaxation time for the crystal, which as for any lossy dielectric is defined as

$$\tau_{RC} = \rho \epsilon_0 \epsilon'_{dc}, \quad (10)$$

where  $\rho$  is the inverse of the conductivity  $\sigma$  displayed in Fig. 6(a) and determined as described in the associated text.

We see there is excellent agreement between these two  $\tau$ 's over four decades of magnitude, and we emphasize that there are no adjustable parameters or model-dependent assumptions entering into these  $\tau$ 's. We interpret this close agreement as showing that the mobile charge redistribution time  $\tau_{RC}$  required for rearrangement of carriers (probably Na<sup>+</sup> and/or Bi<sup>3+</sup> ions) around a given superparaelectric cluster is the relaxation time  $\tau_{pk}$

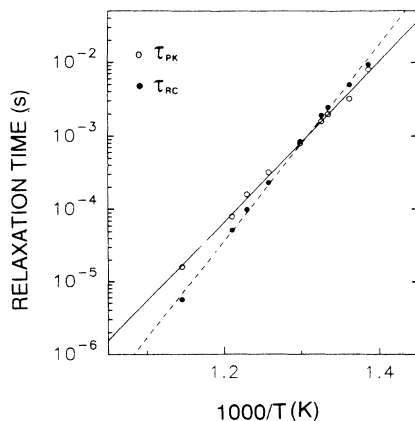


FIG. 10. Relaxation times,  $\tau_{pk}$  and  $\tau_{RC}$  vs  $1000/T$ . The solid and dashed lines are fits of equation  $\tau = \tau_0 e^{W/T}$  with  $\tau_0 = 5.57 \times 10^{-18}$  s,  $W = 25\,090$  K for  $\tau_{pk}$ , and  $\tau_0 = 3.54 \times 10^{-21}$  s,  $W = 30\,720$  K for  $\tau_{RC}$ .

required for the cluster to reorient in the applied electric field. In other words, the cluster is "frozen" against polarization reversal until this charge redistribution can occur. The charge redistribution in turn is influenced by the cluster, as evidenced by the appearance of  $\epsilon'_{dc}$  in Eq. (10) for the charge redistribution time  $\tau_{RC}$ .

The superparaelectric clusters undoubtedly have internal barriers to polarization reversal, as proposed by Cross.<sup>19</sup> He estimated barriers of order 3000 K for larger clusters of volume  $(20 \text{ nm})^3$ . This is an order of magnitude smaller than the energies corresponding to the slopes in Fig. 10, so the internal barriers do not appear to govern the dynamics in the NBT clusters.

The frequency dependence of  $\epsilon'(f, T)$  is illustrated for five temperatures in Fig. 11. The crystal undergoes a relaxation process in the high-temperature region for frequencies below 50 kHz. The solid curves are fits to the Cole-Cole equation:<sup>21</sup>

$$\begin{aligned} \epsilon(f, T) &= \epsilon'(f, T) - i\epsilon''(f, T) \\ &= \epsilon_\infty + \frac{\epsilon_{dc}(T) - \epsilon_\infty}{1 + [i(f/f_0)]^{1-\alpha(T)}}, \end{aligned} \quad (11)$$

where  $\epsilon_{dc}$  and  $\epsilon_\infty$  are the low- and high-frequency limits of the dielectric permittivity,  $\alpha$  is the parameter of the relaxation time distribution, and  $f_0$  is the frequency corresponding to the maximum of  $\epsilon''(f, T)$ . The fits of Eq. (11) to the real part of permittivity with  $\epsilon_\infty = 1280$  are presented in Fig. 11. The parameters from fits at five temperatures shown in Table I indicate a millisecond relaxation time region between 700 and 800 K, which agrees with the data ( $\tau_{pk}$  and  $\tau_{RC}$ ) as shown in Fig. 10. The parameter  $\epsilon_{dc}(T)$  also shows good agreement with the data from extrapolation of Cole-Cole plots (Fig. 7), except at  $T = 650$  K. The relaxation time distribution parameter shows a drop ( $\approx 35\%$ ) around 800 K as temperature increases, which may correspond to the paraelectric to ferroelastic phase transition.<sup>13</sup>

This large frequency-dependent peak shows similarities to behavior in other relaxor ferroelectrics, notably PMN. However, there must be important differences if our

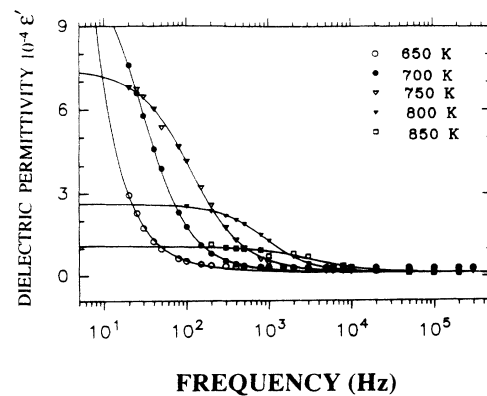


FIG. 11. The real part of dielectric relative permittivity  $10^{-4}\epsilon'$  vs frequency (Hz) at five temperatures. The solid curves are fits of Eq. (11) with parameters of Table I.

TABLE I. The parameters from fits of Eq. (11) to the real part of permittivity ( $\epsilon'$ ) at five temperatures.

	650 K	700 K	750 K	800 K	850 K
$f_0^{-1}$ ( $10^{-3}$ s)	384.7	33.99	8.65	1.12	0.30
$\alpha$	0.104	0.122	0.158	0.103	0.195
$\epsilon_{dc}$	576 000	117 300	74 830	26 290	10 930

above interpretation is correct. In PMN the conductivity is lower at any given temperature [Fig. 5(b)], yet the dispersive dielectric behavior occurs at much lower temperature.<sup>19</sup> Accordingly, the RC relaxation time in PMN is much too long to account for dispersion in the dielectric behavior. Other mechanisms must be operative in PMN, leading to qualitatively different relaxor ferroelectric behavior, as discussed below.

We compared the frequency behavior of the  $\epsilon'$  peak amplitude and the temperature of the  $\epsilon'$  peak position for this high-temperature dielectric anomaly in NBT and for a typical broad dielectric anomaly in PMN.<sup>22-24</sup> The results are shown in Fig. 12. Completely different behavior occurs in NBT and PMN for both the frequency dependences of the peak amplitude [Fig. 12(a)] and the peak position [Fig. 12(b)]. In PMN, the spread of the  $\epsilon'_{max}$  peak values and  $\epsilon'_{max}$  temperatures ( $T_{max}$ ) in different papers is very noticeable.

The broad dispersed maximum of  $\epsilon'$  in PMN is believed to originate in polarization reorientation in microregions with nonzero polarizations. Macroscopic polarization is absent in PMN at these temperatures but polarization fluctuations ( $\langle \Delta P^2 \rangle$ ) are not, as was indicated by the deviation of refractive indexes.<sup>25</sup> The microscopic polarization originates from small regions with  $\langle 111 \rangle$  distortions which begin to develop in PMN below  $\sim 600$  K as evidenced by the behavior of  $\langle \Delta P^2 \rangle$ .<sup>26</sup> Also in NBT there is no evidence for a macroscopic polarization, for  $T > 550$  K (Fig. 3).

What are the origins of these similarities and differences between the high-temperature dielectric anomalies in PMN and NBT? The broad dielectric anomalies characteristic of relaxor ferroelectrics are generally believed to originate in reorientation of small polar regions.<sup>19,27,28</sup> These polar regions are small because they originate from small local inhomogeneities causing strain and electric fields. In PMN the electric fields have been attributed<sup>28</sup> to charges in small regions in which according to transmission electron microscopy the  $Mg^{2+}$  and  $Nb^{5+}$  ions tend to order with a 1:1 ratio rather than the 1:2 ratio required for charge neutrality.<sup>17,29</sup> In NBT there is evidence from Raman scattering<sup>20</sup> for some local 1:1 ordering because the low-frequency Raman results indicate  $Fm3m$  rather than  $Pm3m$  structure. In NBT, however, a 1:1 ratio for ordered  $Na^+$  and  $Bi^{3+}$  cations is stoichiometric and will not cause random electric fields. Instead, we assume local charged regions originating from those  $Na^+$  and  $Bi^{3+}$  cations which are still distributed randomly, with positive and negative charges originating from local excess of  $Bi^{3+}$  and  $Na^+$  ions, respectively, as discussed above.

Accordingly, our assumed random fields in NBT differ

from those assumed by Westphal, Kleeman, and Glinchuk<sup>28</sup> in PMN in two ways; in their origin (random cation placement rather than ordered cation regions) and their time dependence (time-varying rather than quenched).

We now discuss the lower-temperature behavior in the trigonal phase. The evolution to a ferroelectric state in NBT, starting with the onset of the trigonal phase below 640 K, is very close to that in some complex perovskite crystals of the  $AB'_{1/2}B''_{1/2}O_3$  type with an ordered distribution of the  $B'$  and  $B''$  ions. In highly ordered  $PbYb_{1/2}Ta_{1/2}O_3$  (PYT) a recent study<sup>16</sup> showed successive paraelectric-antiferroelectric-ferroelectric phase transitions. Both NBT and PYT have two similar states which exhibit normal (ferroelectric) and double (antiferroelectric) electrical hysteresis loops at different temperature regions. The low-temperature phase (ferroelectric) is characterized by a small inflection-point-type anomaly in  $\epsilon'(f, T)$ . Both compounds also have another anomaly of the  $\epsilon'$  peak type at higher temperatures (640 K in NBT,

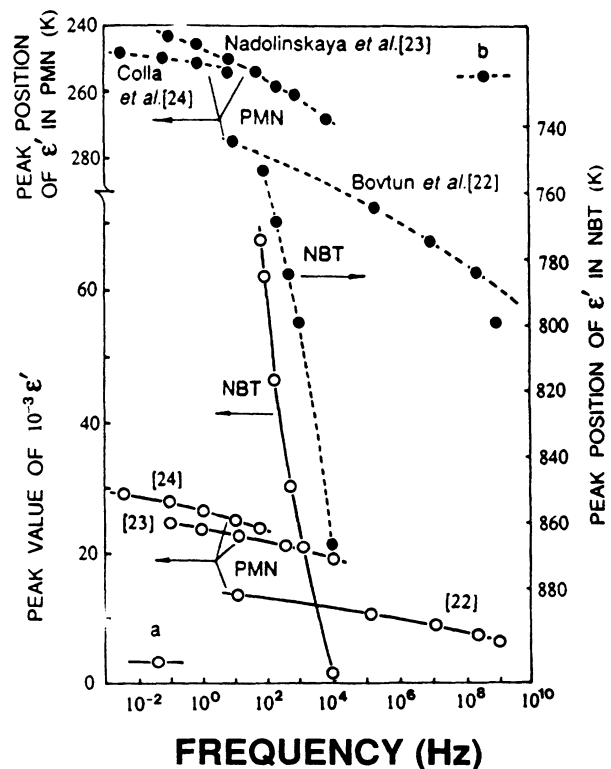


FIG. 12. (a) The frequency dependence of  $\epsilon'$  peak values for PMN and NBT. (b) The frequency dependences of  $\epsilon'$  peak positions for PMN and NBT.

see Sec. III A). An identical pattern of evolution through these phases is also found from dielectric measurements for  $\text{PbCo}_{1/2}\text{W}_{1/2}\text{O}_3$  (PCW).<sup>14,15</sup> Moreover, an advanced transmission electron microscopy (TEM) study of PCW has revealed evidence for more complicated evolution through a new type of "antiferroelectric incommensurate" phase transition.<sup>30</sup> This study has found a direct interaction between the antiferroelectric domains and the incommensurate structure that implies a significant effect of pinning in the behavior of most physical parameters. We speculate that this evidence from PYT and PCW also favors the existence of an antiferroelectric incommensurate phase in NBT, between the *A* and *B* dielectric anomalies.

Some unusual properties of NBT in this temperature region find their explanation in the framework of our supposition. For example, the time effects in the behavior of the dielectric constant (decrease or increase of  $\epsilon'$  by a few percent with time constants of order 1 h) occur just in this region *A*.<sup>10</sup> It is well known that time dependences of this kind are characteristic features of commonly observed incommensurate phases.<sup>31</sup> Also, the specific thermal hysteresis in the  $\epsilon'$  behavior (Fig. 2) appears similar to a thermal hysteresis found in the incommensurate phases of many incommensurate systems.<sup>31</sup> In PCW, the highest dielectric anomaly occurs at the commensurate (paraelectric)-incommensurate (antiferroelectric) transition and the anomaly at the next "lock-in" transition to the commensurate ferroelectric phase is small, whereas only the "lock-in" phase transition is accompanied by a significant anomaly in common incommensurate crystals. In NBT also, the higher (640 K) transition has the larger dielectric anomaly. According to a recent study,<sup>30</sup> the symmetry for an antiferroelectric phase in PCW is suggested to be monoclinic or triclinic. If this is true for NBT also, the low-symmetry phase can permit the rotation of optical indicatrices observed in microdomains<sup>8</sup> which has been a puzzle in the case of trigo-

nal symmetry. Perhaps NBT has such microdomains within a trigonal matrix which has the symmetry seen in neutron-diffraction experiments.<sup>13</sup>

## V. CONCLUSIONS

Between 900 and 600 K we have found a new, very large low-frequency permittivity peak in NBT. This dielectric behavior is explainable in terms of superparaelectric clusters existing in the tetragonal phase. The frequency dependence of the response of these clusters appears to be governed by the "RC" relaxation time required for carriers to redistribute, allowing local fields to change and thus allowing reversal of the superparaelectric dipole moments.

Below 640 K, NBT shows a tandem of phase transitions similar to that exhibited by some related ordered crystals. The upper transition is from a superparaelectric tetragonal to an antiferroelectric or incommensurate trigonal phase, while the lower transition is to a ferroelectric phase of trigonal structure.

Further study by NMR, Brillouin, surface science, and other techniques is needed to better determine the local atomic arrangements in the various phases, and the nature (antiferroelectric or incommensurate) of the intermediate phase. Particularly desirable is extension of dielectric measurements to the lowest possible frequencies, to extend to lower temperatures our knowledge of the dc response of the superparaelectric dipole moments.

## ACKNOWLEDGMENTS

The authors express sincere thanks to T. V. Kruzina for single-crystal growth and to Professor George F. Tuthill for helpful discussions. This work was supported in part by NSF Grant No. DMR-9017429, DOE Equipment Grant No. FG05-91ER79046, a NASA EPSCoR Grant, and an NRC CAST Grant.

\*Present address: A.F. Ioffe Physical Technical Institute, Russian Academy of Science, St. Petersburg 194021, Russia.

<sup>1</sup>G. A. Smolensky, V. A. Isupov, A. I. Agranovskaya, and N. N. Krainik, *Fiz. Tverd. Tela (Leningrad)* **2**, 2982 (1960) [*Sov. Phys. Solid State* **2**, 2651 (1961)].

<sup>2</sup>K. Sakata and Y. Masuda, *Ferroelectrics* **7**, 347 (1974).

<sup>3</sup>I. P. Pronin, P. P. Syrnikov, V. A. Isupov, and G. A. Smolensky, *Pis'ma Zh. Tekhn. Fiz.* **5**, 705 (1979) [*Sov. Tech. Phys. Lett.* **5**, 289 (1979)].

<sup>4</sup>I. P. Pronin, P. P. Syrnikov, V. A. Isupov, V. M. Egorov, and N. V. Zaitseva, *Ferroelectrics* **25**, 395 (1980).

<sup>5</sup>I. P. Pronin, N. N. Parfenova, N. V. Zaitseva, V. A. Isupov, and G. A. Smolensky, *Fiz. Tverd. Tela (Leningrad)* **24**, 1860 (1982) [*Sov. Phys. Solid State* **24**, 1060 (1982)].

<sup>6</sup>J. A. Zvirgzds, P. P. Kapostins, J. V. Zvirgzde, and T. V. Kruzina, *Ferroelectrics* **40**, 75 (1982).

<sup>7</sup>V. A. Isupov and T. V. Kurzina, *Izv. AN SSSR, Ser. Fiz.* **47**, 616 (1983) [*Sov. Phys.: Bull. Acad. Sci. USSR, Phys. Ser.* **47**, 194 (1983)].

<sup>8</sup>V. A. Isupov, I. P. Pronin, and T. V. Kruzina, *Ferroelectrics Lett.* **2**, 205 (1984).

<sup>9</sup>S. B. Vakhruшев, V. A. Isupov, B. E. Kvyatkovsky, N. M.

Okuneva, I. P. Pronin, G. A. Smolensky, and P. P. Syrnikov, *Ferroelectrics* **63**, 153 (1985).

<sup>10</sup>K. Roleder, J. Suchanicz, and A. Kania, *Ferroelectrics* **89**, 1 (1989).

<sup>11</sup>J. Suchanicz and W. S. Ptak, *Ferroelectrics Lett.* **12**, 71 (1990).

<sup>12</sup>J. Suchanicz and V. S. Ptak, *Izv. Akad. Nauk SSSR, Ser. Fiz.* **555**, 136 (1991) [*Bull. Acad. Sci. USSR, Phys. Ser.* **55**, 136 (1991)].

<sup>13</sup>S. V. Vakhruшев, B. E. Kvyatkovsky, R. S. Malysheva, N. M. Okuneva, E. L. Plachenova, and P. P. Syrnikov, *Kristallografiya* **34**, 154 (1989) [*Sov. Phys. Crystallogr.* **34**, 89 (1989)].

<sup>14</sup>V. A. Bokov, S. A. Kizhaev, I. E. Mylnikova, and A. G. Tutov, *Fiz. Tverd. Tela (Leningrad)* **6**, 3038 (1964) [*Sov. Phys. Solid State* **6**, 2419 (1965)].

<sup>15</sup>K. Uchino and S. Nomura, *Ferroelectrics* **17**, 505 (1978).

<sup>16</sup>N. Yasuda and J. Konda, *Appl. Phys. Lett.* **62**, 535 (1993).

<sup>17</sup>K. Z. Baba-Kishi and D. J. Barber, *J. Appl. Cryst.* **23**, 43 (1990).

<sup>18</sup>M. E. Lines and A. M. Glass, *Principles and Applications of Ferroelectrics and Related Materials* (Clarendon, Oxford, 1977).

- <sup>19</sup>L. E. Cross, *Ferroelectrics* **76**, 241 (1987).
- <sup>20</sup>I. G. Siny, T. A. Smirnova, and T. V. Kruzina, *Fiz. Tverd. Tela (Leningrad)* **33**, 110 (1991) [*Sov. Phys. Solid State* **33**, 61 (1991)]; *Ferroelectrics* **124**, 207 (1991).
- <sup>21</sup>V. V. Daniel, *Dielectric Relaxation* (Academic, London, 1967).
- <sup>22</sup>V. P. Bovtun, N. N. Krainik, L. A. Markova, Yu. M. Poplavko, and G. A. Smolensky, *Fiz. Tverd. Tela (Leningrad)* **26**, 378 (1984) [*Sov. Phys. Solid State* **26**, 225 (1984)].
- <sup>23</sup>E. G. Nadolinskaya, N. N. Krainik, A. V. Shilnikov, G. A. Smolensky, and L. Kh. Vologirova, *Fiz. Tverd. Tela (Leningrad)* **29**, 3368 (1987) [*Sov. Phys. Solid State* **29**, 1932 (1987)].
- <sup>24</sup>E. V. Colla, E. Yu. Koroleva, N. M. Okuneva, and S. B. Vakhyshev, *J. Phys.: Condens. Matter* **4**, 3671 (1992).
- <sup>25</sup>G. Burns and F. H. Dacol, *Solid State Commun.* **48**, 853 (1983).
- <sup>26</sup>N. de Mathan, E. Husson, G. Calvarin, J. R. Gavarri, A. W. Hewat, and A. Morell, *J. Phys.: Condens. Matter* **3**, 8159 (1991).
- <sup>27</sup>D. Viehland, M. Wittig, and L. E. Cross, *Ferroelectrics* **120**, 71 (1991).
- <sup>28</sup>V. Westphal, W. Kleemann, and M. D. Glinchuk, *Phys. Rev. Lett.* **68**, 847 (1992).
- <sup>29</sup>A. D. Hilton, D. J. Barber, C. A. Randall, and T. R. Shrout, *J. Mater. Sci.* **25**, 3461 (1990).
- <sup>30</sup>C. A. Randall, S. A. Markgraf, A. S. Bhalla, and K. Baba-Kishi, *Phys. Rev. B* **40**, 413 (1989).
- <sup>31</sup>K. Hamano, in *Incommensurate Phases in Dielectrics*, edited by R. Blinc and A. P. Levanyuk (North-Holland, Amsterdam, 1986), Vol. 1, Chap. 9.